Calculated and Measured Emittance of a Sputter-Type Negative-Ion Source

James H. Billen

November 1982

UWFDM-491

Invited paper presented at the Seventh Conference on the Application of Accelerators in Research and Industry, Denton, Texas, November 8–10, 1982.

FUSION TECHNOLOGY INSTITUTE

UNIVERSITY OF WISCONSIN

MADISON WISCONSIN

Calculated and Measured Emittance of a Sputter-Type Negative-Ion Source

James H. Billen

Fusion Technology Institute
University of Wisconsin
1500 Engineering Drive
Madison, WI 53706

http://fti.neep.wisc.edu

November 1982

UWFDM-491

Invited paper presented at the Seventh Conference on the Application of Accelerators in Research and Industry, Denton, Texas, November 8–10, 1982.

CALCULATED AND MEASURED EMITTANCE OF A SPUTTER-TYPE NEGATIVE-ION SOURCE

James H. Billen

Fusion Engineering Program
Nuclear Engineering Department
University of Wisconsin-Madison
Madison, Wisconsin 53706

November 1982

UWFDM-491

Invited paper presented at the Seventh Conference on the Application of Accelerators in Research and Industry, Denton, Texas, Nov. 8-10, 1982.

CALCULATED AND MEASURED EMITTANCE OF A SPUTTER-TYPE NEGATIVE-ION SOURCE

James H. Billen
Dept. of Nuclear Engineering and Dept. of Physics
University of Wisconsin
Madison, Wisconsin 53706

Summary

A method for calculating the beam current and emittance of a negative ion beam from a sputter-type source is described. Calculations are compared to measured emittance. The dependence of the emittance on ion source parameters such as cathode shape, exit aperture diameter, and cathode voltage is discussed.

Introduction

Earlier I reported[1] results of ion trajectory calculations that correctly predict the erosion pattern of the sputter cathode in the Wisconsin Source of Negative Ions by Cesium Sputtering (SNICS) and similar sources. Based upon results of our Cs^+ trajectory calculations we modified the original SNICS geometry to deliver 100% of the available Cs^+-ion current onto the cathode face, eliminating the unwanted sputtering of the side of the cylindrical cathode. With the initial successes in predicting observed erosion rates and in improving ionizer efficiency we took on the somewhat more ambitious task of modelling the negative-ion beam characteristics. Specifically one would like to calculate both the negative-ion beam current and emittance for various choices of cathode voltage, exit aperture diameter, cathode shape, and perhaps other electrode configurations.

Procedure

The procedure we developed to accomplish this task involves four steps: 1) calculation of the electric potential for a chosen source geometry and cathode voltage, 2) calculation of the Cs^+ ion trajectories to determine the cathode sputter rate, 3) calculation of the negative ion trajectories emerging from the cathode surface, and 4) construction of the phase space brightness distribution from the final positions and velocities of the negative ions. The emittance and beam current may then be determined from the brightness distribution. Reference 1 describes in detail the first two steps in the process. Figure 1 shows equipotentials for the SNICS geometry now in use and Fig. 2 illustrates some sample Cs^+ trajectories. For the present problem we calculate some 1250 Cs^+ ion trajectories emerging from the hot W ionizer with an initial energy of about 0.15 eV.

The third step traces a large number of negative-ion trajectories evenly distributed over all possible initial positions, directions, and energies. We imagine each negative-ion trajectory to be a beamlet which will contribute a certain amount of current to a region of phase space as the beamlet emerges from the source exit aperture. The magnitude of this current depends on many factors and includes all three of the trajectory's initial parameters, the cathode material, and the incident Cs^+ ion current and energy. Negative ion sputter yields are very sensitive to surface conditions such as Cs^o coverage. Some data exist on the total sputter yield for many materials[2] but little information is available on the fraction of negative ions in the total sputter yield. The negative-ion beam current is proportional to the product of the negative ion fraction f^- and the incident Cs^+ current I_{Cs}. The current I_{Cs} is also difficult to determine experimentally since the sputter cathode supply current includes secondary electrons and negative ions emitted from the cathode surface in addition to the Cs^+ current. We arbitrarily chose 0.1 mA for the product f^-I_{Cs} for a basis of comparison among different geometries. Combining experimental results for Ni^- beams from SNICS with the calcu-

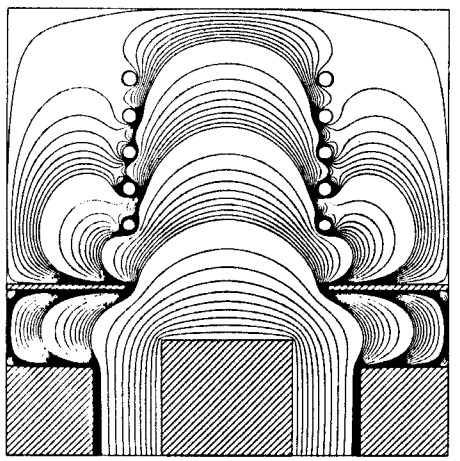

Figure 1. Equipotentials for the SNICS geometry currently in use. The cathode at lower center is several kV negative with respect to the ionizer and housing.

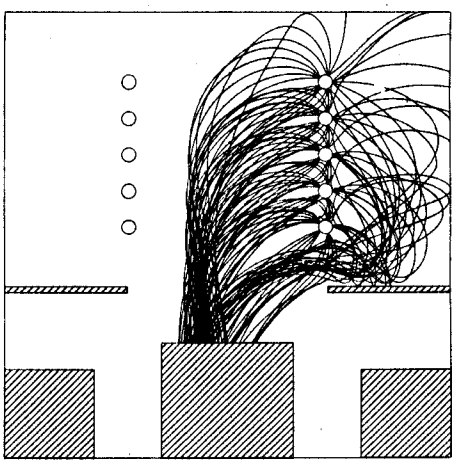

Figure 2. Sample Cs^+ ion trajectories. One-tenth of the 1250 calculated trajectories appear here emerging from the 1-mm diameter hot W filament.

lation results indicates that f^- is typically about 2%. Thus the Ni^- beam currents reported below correspond to a Cs^+ current of roughly 5 mA. For the purposes of this calculation the current in each beamlet also includes the effects of 1) the sputter rate of the cathode surface at the beamlet's point of origin, 2) the spectrum of initial sputtered particle energies E_i, and 3) the angle of emission ϕ_i with respect to the local surface normal direction.

The cathode sputter rate itself includes the dependence on Cs^+ energy (i.e. cathode voltage) for any one of several materials[2] and the $(\cos\theta)^{-5/3}$ dependence[3] for incident angles $\theta \lesssim 70°$. For few-keV heavy particles incident on metal surfaces the sputtered particles emerge with a $\cos\phi_i$ distribution[4] and with an energy spectrum that peaks near 20 eV but which extends to at least 100 eV.[5,6] For a meaningful sampling of the initial parameters that influence the current of each beamlet we typically trace negative-ion trajectories from 50 positions with 20 different energies E_i and 19 angles ϕ_i, a total of 19000 trajectories.

The fourth step of the procedure is the construction of the phase space brightness distribution from the negative-ion trajectories. In cylindrical coordinates each beamlet has an initial position (r_i,θ_i,z_i), an initial velocity $(\dot{r}_i,\dot{\theta}_i,\dot{z}_i)$, a final position (r_f,θ_f,z_f), and a final velocity $(\dot{r}_f,\dot{\theta}_f,\dot{z}_f)$. We define a primary trajectory as one with $\theta_i=0$ and $\dot{\theta}_i=0$. The 19000 trajectories described above are primary trajectories that all lie in the same (r,z) plane. Cylindrical symmetry permits calculation of the resultant 2-dimensional phase space coordinates for any trajectory with the same initial position (r_i,z_i), energy E_i and angle ϕ_i as the corresponding primary trajectory. Thus for each beamlet whose end point falls within the diameter of the source exit aperture we generate the phase space coordinates of 400 beamlets evenly distributed over all possible θ_i and $\dot{\theta}_i$. Each of these beamlets contributes an identical current to its respective location in phase space.

By convention the r axis is the x axis of rectangular coordinates when $\theta=0$. Primary trajectories, therefore, lie in the (x,z) plane. The position and divergence coordinates in the (x,x') phase plane of a beamlet at the source exit aperture are $x=r_f$ and $x'=r_f'\equiv\tan^{-1}(\dot{r}_f/\dot{z}_f)$. In a cylindrically symmetric potential $\dot{\theta}$ is a constant, so the final azimuthal angle coordinate of any trajectory is

$$\theta_f = \theta_i + \dot{\theta}_i\tau$$

where τ is the elapsed time of the particle trajectory from cathode to exit aperture. Hence a trajectory with nonzero θ_i and $\dot{\theta}_i$ has (x,x') phase space coordinates $(r_f\cos\theta_f, r_f'\cos\theta_f)$ where (r_f,r_f') is the location of the corresponding primary trajectory.

The computer code accumulates the beam current of each beamlet into a 50 × 50 array of cells that covers the positive-position half of the (x,x') phase plane. Each cell has an area of about 0.5 mm mrad. After the current from all beamlets has been added to the phase space distribution the program averages the current at each cell location. An averaging window of about 10 mm mrad for few-keV beams at the source exit aperture simulates the phase space resolution of our emittance measuring device. (This system[7] continuously samples a parallelogram-shaped phase space area extending over 1 mm × 2.8 mrad after the beam has been accelerated to 30-40 keV.) The resulting current in each cell is proportional to the local brightness B(x,x'). A given fraction of the maximum brightness defines a contour in phase space whose enclosed phase space area A and current may be determined directly from the accumulated array. The normalized emittance is $(A/\pi)E^{1/2}$ where E is the energy of the beam emerging from the source aperture.

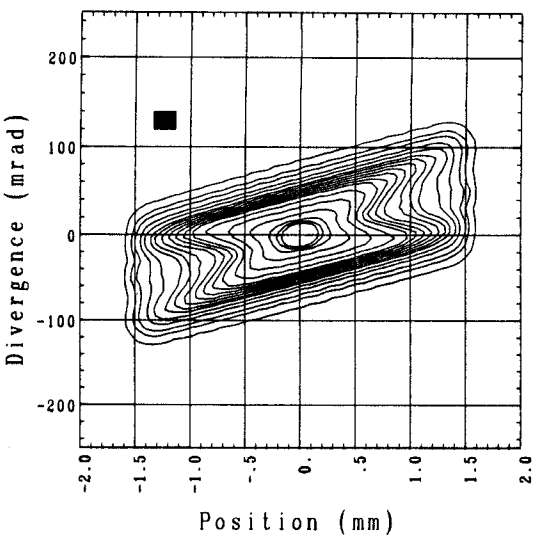

Figure 3. Calculated phase space contours of equal brightness for a 2.4-kV Ni^- beam. The 6th contour from the outside corresponds to 4.2% of the maximum brightness and encloses 90% of the total beam current.

Results

Figure 3 shows contours of equal brightness for a 2.4-keV Ni^- beam emerging from a 3-mm diameter aperture. The solid curve in Fig. 4 plots the normalized emittance for these contours as a function of the fraction of the total beam current they enclose. The individual points are measurements that were made shortly after the installation of a new flat cathode before any appreciable erosion of the surface. The calculation is in reasonable agreement with experiment though it slightly over-estimates the emittance for contours enclosing less than 80% of the beam and underestimates it above 90%.

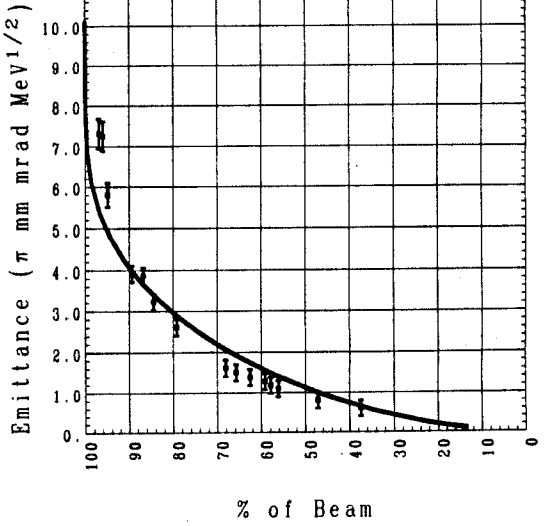

Figure 4. Normalized emittance vs. the percent of beam current enclosed by the contours in Fig. 3. The curve is a calculation and the points are measurements for the same operating conditions as the calculation.

Effects of Cathode Erosion

One of the first things we investigated with the computer model was the effect of an eroded hole in the sputter cathode. We had observed experimentally a gradual increase in the beam emittance with running time and had speculated that the increase was caused by the changing shape of the cathode surface since we could not detect appreciable changes in any other source operating parameters. This is indeed the case.

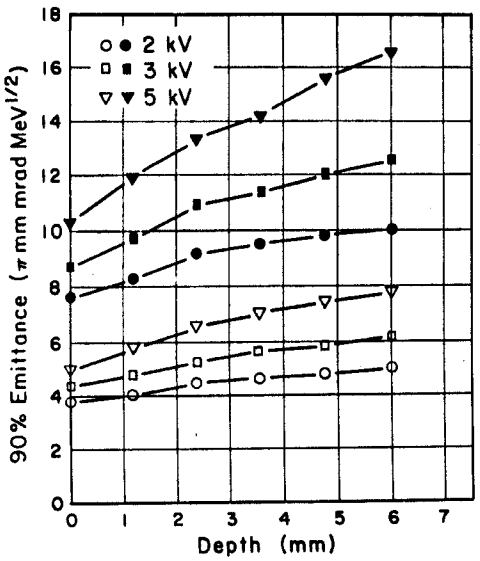

Figure 5. Normalized emittance for 90% of the beam vs. the depth of an eroded hole in an initially flat sputter cathode. Open symbols refer to a 3.0-mm diameter exit aperture and solid symbols to a 6.35-mm diameter aperture.

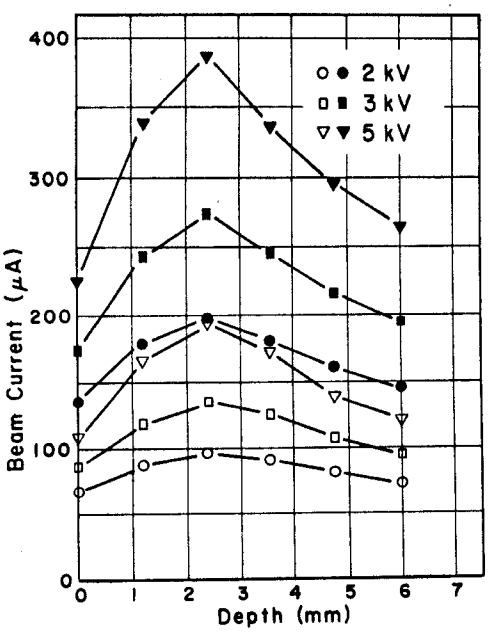

Figure 6. Calculated beam current that has the emittance shown in Fig. 5. The calculation assumed a 5-mA incident Cs^+ beam, sputter rates for nickel, and that 2% of the sputtered particles emerge as negative ions.

We calculated phase space distributions for several cathodes with various depths of an eroded hole whose shape closely matched that of a used sputter cathode. Figure 5 shows the emittance and Fig. 6 the beam current versus the depth of the hole for several cathode voltages and for two exit aperture diameters. The emittance does increase slowly as the hole deepens. The initial rise followed by a more gradual decline in beam current with increasing erosion also agrees qualitatively with observed source behavior. While the current peaks near 2.5-mm hole depth the average brightness (current divided by the square of emittance) reaches a maximum for about 1.5 mm depth. For either of the two aperture diameters the average brightness is slightly higher for lower cathode voltage. However, the beam through a 3-mm diameter aperture has twice the average brightness of a beam through a 6.35-mm aperture.

Other Cathode Shapes

We have investigated other cathode shapes as well. A cathode with a spherically concave surface whose radius of curvature approximately equals the distance between the cathode and the exit aperture yields a higher beam current but at the expense of somewhat increased emittance. For a 2-kV cathode the spherically dished cathode produces 36% more beam current with 17% higher emittance than a flat cathode. The average brightness does not change. As the cathode voltage increases the current for a spherically dished cathode increases faster than for a flat cathode. At 5 kV the current is 60% larger and the emittance is 27% larger than for a flat cathode. The average brightness at 5 kV for both shapes is nearly the same and only slightly less than the brightness for 2-kV cathodes.

Figure 2 illustrates that the Cs^+ beam illuminates only a 7.0-mm diameter area on the 9.5-mm diameter cathode. If one reduces the cathode diameter to 6.35 mm the calculation shows that the entire Cs^+ ion current still falls on the face of the cathode. In other words the same Cs^+ current illuminates a somewhat smaller area of 6.35 mm diameter compared to 7.0 mm with the larger cathode. One might, therefore, expect a beam of essentially the same intensity but with improved emittance because of the smaller source area. However, the same radial component of the electric field that forces the Cs^+ beam into a smaller diameter also pushes the negative ions radially outward. The net effect is a decrease in both beam current and emittance. The beam current from the smaller cathode is lower by 16% and the emittance is lower by 13%. The effect is approximately independent of cathode voltage and leads to an increase of about 12% in the average brightness.

Effects of Aperture Diameter

The calculation predicts a linear increase in both the beam current and the emittance for a fixed cathode voltage. We have not made extensive measurements with different aperture diameters since it requires irreversible modification of our present source. However, the source initially had a 1.6 mm aperture that we enlarged to 2.25 mm and later to 3.0 mm. Emittance measurements with these sizes for the exit aperture agree with the prediction for cases where other operating conditions were well enough characterized for a comparison. Figure 7 shows that the average brightness for 90% of the beam falls as the reciprocal of the aperture diameter. The curve corresponds to a 5-kV nickel cathode with a flat surface, and it is characteristic of all cases we have calculated so far. The width in the divergence coordinate of the phase space distribution (see Fig. 3) is nearly constant so that increasing the aperture diameter merely lengthens the distribution in the position coordinate.

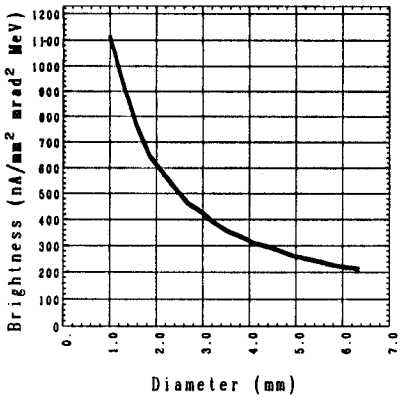

Figure 7. Normalized brightness for 90% of the beam vs. the diameter of the source exit aperture. Normalized brightness is $I/(\pi\bar{E})^2$ where I is the beam current and $\bar{E}$ is the normalized emittance. The curve is for a 5-kV nickel cathode. The shape of the brightness curve results from the fact that both I and $\bar{E}$ increase in direct proportion to the aperture diameter.

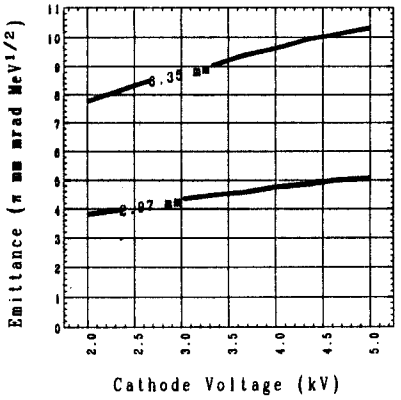

Figure 8. Normalized emittance for 90% of the beam vs. cathode voltage for two sizes of the exit aperture.

Effects of Cathode Voltage

If one were to neglect the energy spectrum of the sputtered particles, say by assuming their initial energy to be zero, then the shape of the phase space distribution at the source exit aperture would be independent of the cathode voltage. This independence results from the fact that the paths of a given ion in different potentials are the same. The ion energy along the path scales as the potential. Thus sputtered particles of zero initial energy would exhibit an increase in the normalized emittance exactly as the square root of the cathode voltage because of the factor $E^{1/2}$ in converting phase space area to normalized emittance. When one includes the effect of the nonzero initial energy of the sputtered particles the phase space distribution for lower cathode voltages tends to spread out more than for higher voltages. The normalized emittance then depends less strongly than the 0.5 power of the cathode voltage. The emittance curves in Fig. 8 for a flat cathode increase approximately as $V^{0.31}$. Nonzero sputtered particle energies increase the emittance at all voltages, but the increase is worse (i.e. larger) for lower cathode voltages. All of the results discussed below include the effect of the sputtered particle energy distribution.

Cathode shapes that tend to focus the negative ions produce higher beam currents but they also influence the emittance as a function of cathode voltage. For the spherically dished cathode described above the emittance increases as $V^{0.40}$ compared to $V^{0.31}$ for a flat cathode. The situation becomes rather complicated as a hole erodes in the cathode surface. The deeper the eroded hole the more rapidly the emittance rises with voltage. The effect is illustrated in Fig. 5. The gap between the curves for different cathode voltages widens as the hole depth increases. For a 2.4-mm hole depth and a 3-mm aperture the emittance (in π mm mrad $MeV^{1/2}$) is given by the empirical relation $3.27\ V^{0.43}$ where V is in kV. When the hole depth increases to 6.0 mm the relation is $3.59\ V^{0.48}$. The exact shape of a cathode at the time of an emittance measurement is impossible to determine. However, careful measurements of the emittance at different cathode voltages during which other operating conditions were held constant always showed a voltage dependence within the range of the calculations.

For the nickel cathode we have been considering the calculated beam current rises even more rapidly with cathode voltage than the emittance does. This results in an average brightness that is almost independent of the cathode voltage. The increase in current results almost entirely from the increased sputter yield for nickel as a function of the Cs^+-ion bombarding energy. The results for current and brightness will, of course, be different for materials with a different energy dependence of the sputter rate. Only one set of negative ion trajectories need be calculated to investigate other ions or voltages. Using appropriate scaling operations the computer code will upon request calculate the emittance and current for any other ion or potential.

Conclusion

A very simple model in which only electrostatic forces play a role correctly describes a wide variety of the negative-ion beam characteristics for SNICS and similar sputter-type sources. The calculations serve as a useful tool in the continuing development of the ion source, particularly for optimizing the beam emittance.

Acknowledgements

I wish to thank S. Riedhauser, G.T. Caskey, D.B. Bullen and D. Wiltzius for their suggestions and helpful discussions. I am also grateful to Lori Wong of the National Magnetic Fusion Energy Computing Center for her assistance with the computer generated graphics. This work was supported by the U.S. Dept. of Energy.

References

1. J.H. Billen, Proc. 3rd Int. Conf. of Electrostatic Accelerator Technology (Oak Ridge, Tenn. 1981) 238.
2. H.H. Andersen and H.L. Bay in *Topics in Applied Physics*, Vol. 47 (R. Behrisch, ed. 1981) 145.
3. P. Sigmund, Phys. Rev. 184 (1969) 383.
4. M. Kaminsky, *Atomic and Ionic Impact Phenomena on Metal Surfaces* (Academic Press, N.Y. 1965) 169.
5. V.I. Veksler, Soviet Physics JETP 11 (1960) 235.
6. A.R. Krauss and D.M. Gruen, Nucl. Instr. and Meth. 149 (1978) 547.
7. L.L. Ames, Nucl. Instr. and Meth. 151 (1978) 363.